JCTC Journal of Chemical Theory and Computation

Article

pubs.acs.org/JCTC

Electroluminescence in Molecular Junctions: A Diagrammatic Approach

Himangshu Prabal Goswami,*[,†] Weijie Hua,[‡] Yu Zhang,[‡] Shaul Mukamel,[‡] and Upendra Harbola*[,†]

[†]Department of Inorganic and Physical Chemistry, Indian Institute of Science, Bangalore 560012, India

[‡]Department of Chemistry, University of California, Irvine, California 92697-2025, United States

ABSTRACT: We compute electroluminescent signal in a current carrying single molecule junction using a superoperator formalism. Liouville space loop diagrams are used to identify all density matrix pathways that emit photons via the electroluminescence process. A frequency resolved spectrum is expressed in terms of the various Fock space states of the isolated molecule that participate in the creation and subsequent recombination of exciton. Application is made to a multilevel Coulomb blockade model system and to a gold−benzene-1,4-dithiol−gold molecular junction.

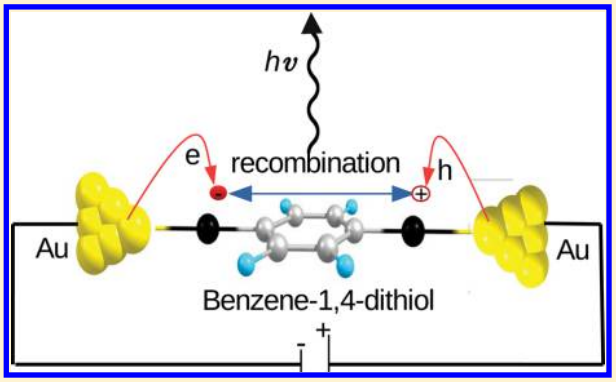

I. INTRODUCTION

Molecular junctions are important examples of open quantum systems[1,2] that may consist of a single simple or complex molecule or a quantum dot. A single molecule break junction or a single molecule sandwiched between a scanning tunneling microscopy (STM) tip and metal surface are well-known examples of molecular junctions. They have potential applications to single molecular electronic devices.[3] Recently optical spectroscopy of molecular junctions has become an active area of research.[4−15] Since molecular junctions are in a current carrying state, its optical response differs from that of an isolated molecule.[16] The conduction properties of a molecular junction are significantly affected by the configuration of the molecule. It is therefore important to understand both the electric and optical responses of the junction so as to fully characterize the dynamics.

Theoretical formalism of molecular junctions must be based on a quantum description of the detected field. Usually the signal is evaluated directly by doing a perturbation in the molecule−field interaction.[17−20] The effect of the leads may be treated within the quantum master equation (QME)[21] (weak molecule−lead coupling) or using the nonequilibrium Greens function (NEGF) formalism.[22,23] Several processes such as current induced fluorescence,[24] spontaneous and stimulated Raman signals,[21] and inelastic electron tunneling[25] have been theoretically studied previously in the single molecule junctions. Recently, we presented a diagrammatic method[21] to study the optical response of a single molecule junction based on loop diagrams combined with the quantum master equation formalism. These loop diagrams describe the time evolution of the density matrix which happens through various Liouville space pathways.[17] In this work we adopt the Liouville space loop diagrammatic method to study electroluminescent signals from molecular junctions.

In a molecular junction, the molecule continuously exchanges electrons with the leads (electronic reservoirs) creating excitons (electron−hole pair) in the molecule which radiatively recombine, leading to the phenomenon of electroluminescence. Electroluminescence is the basic process in light emitting diodes (LED)[26] that can be made of both organic polymers[27] and quantum dots.[28] Single molecule electroluminescence has been realized in the core-substituted naphthalenediimide molecules entrapped between two metallic single-walled carbon nanotube electrodes[29] and perylene adsorbed on silicon carbide probed by scanning tunneling microscopy.[30] STM tips have also been used as a source of electron injectors to study electroluminescence in several systems such as graphene, carbon nanotubes,[31−33] and conjugated polymer chain between a Au(111) surface and STM tip.[34]

Within a QME or NEGF approach, the molecule−lead interaction is treated nonperturbatively. This renders it difficult to distinguish between electroluminescence and other spontaneous light emission processes since all such processes happen simultaneously. The distinction can be made very easily by doing a perturbation directly on the molecule−lead coupling. Electroluminescence involves the injection of an electron and a hole from the leads to the molecule, and the signal therefore requires at least fourth-order perturbation in the molecule−lead coupling. In this work we present a microscopic calculation of electroluminescence signal at single molecular junctions based on perturbation theory.

Received: May 27, 2015
Published: August 3, 2015

DOI: 10.1021/acs.jctc.5b00500
J. Chem. Theory Comput. 2015, 11, 4304−4315

The loop diagrams that contribute to the formation of an exciton and the subsequent optical detection can be intuitively drawn. The diagrams represent the several pathways by which a signal can be obtained. We account for the electroluminescent signal by considering the rate of change of photon occupation in the detected mode as a perturbation in the molecule−field and molecule−lead coupling and then combine it with the many-body states (Fock states) of the isolated molecule. The loop diagrams clearly show how various molecular states (neutral or charged) are involved during the process. Hence the computation is based on the isolated molecule's Fock states which can be obtained with standard quantum chemistry calculations. Interpretation of these diagrams is based on Liouville space superoperator algebra.[35] We present a set of rules that can be used to read the electroluminescent signal directly from the diagrams. We apply these rules to a generic multilevel Coulomb blockade model and a gold−benzene-1,4-dithiol−gold molecular junction to compute the signal.

This work is organized as follows. In the next section, section II, we introduce the Hamiltonian and formulate electroluminescence in terms of Liouville space loop diagrams. In section III, we use Liouville space superoperator formalism to evaluate the electroluminescence signal perturbatively. We discuss rules to read the diagrams and write down the algebraic expression for the signal directly from the loop diagrams. In section IV, we apply these rules to evaluate the electroluminescent spectrum in a multilevel Coulomb blockade model system. In section V, we evaluate the electroluminescence signal from a benzene-1,5-dithiol molecular junction coupled to two gold leads. We conclude in section VI.

II. DIAGRAMMATIC FORMULATION OF ELECTROLUMINESCENCE IN MOLECULAR JUNCTIONS

Consider a molecule sandwiched between two metal contacts (leads) or an STM tip and a metal surface. A manifold of many-body states (neutral or charged) with different oxidation states can participate in the electron transfer process between the molecule and leads. Electron exchange may occur either from the ground states of the neutral molecule or the charged molecule. This leads to excitations in the molecule. This may induce transfer of an electron or a hole or both (Figure 1). Transfer of electrons and holes leads to the creation of excitons in the molecular junction. Radiative recombination of excitons created by the charge current gives rise to electroluminescence.

The molecule−lead Hamiltonian can be written as $\hat{H} = \hat{H}_o + \hat{H}_{int}$

$$\hat{H}_o = \hat{H}_m + \hat{H}_f + \hat{H}_x \tag{1}$$

$$= \hat{H}_m + \epsilon_f \hat{a}_f^\dagger \hat{a}_f + \sum_{x\in l,r} \epsilon_x \hat{c}_x^\dagger \hat{c}_x \tag{2}$$

$$\hat{H}_{int} = \hat{H}_{ml} + \hat{H}_{mf} \tag{3}$$

Here $\hat{H}_m$, $\hat{H}_f$, and $\hat{H}_x$ are the molecular, the radiation field, and the lead Hamiltonians, respectively. $\hat{H}_{ml}$ and $\hat{H}_{mf}$ are the molecule−lead coupling and molecule−field interaction Hamiltonians, respectively, defined as

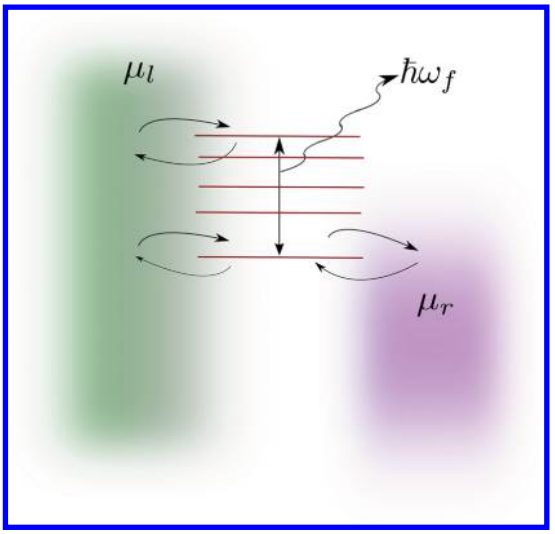

Figure 1. Orbital scheme in a molecular junctions. The orbitals are shown as horizontal lines which are coupled to leads at chemical potentials μ_l and μ_r. The arrows show possible electron and hole exchange processes. $\hbar\omega_f$ is the energy of a spontaneously emitted electroluminescence photon.

$$\hat{H}_{ml} = \sum_{x,s} (T_{sx}\hat{c}_s^\dagger \hat{c}_x + T_{sx}^* \hat{c}_x^\dagger \hat{c}_s) \tag{4}$$

$$\hat{H}_{mf} = \hat{\mathcal{E}}_f(t)\, \hat{V}^\dagger(t) + \hat{\mathcal{E}}_f^\dagger(t)\, \hat{V}(t) \tag{5}$$

The molecular Hamiltonian need not be specified at this point and may contain many-body effects, e.g., electron−electron and electron−phonon interactions. $\hat{\mathcal{E}}_f(r,t) = E_f(r,t)\, \hat{a}_f(t)$ represents the complex amplitude of the field, and $E_f(r,t)$ is the envelope of the field. $\hat{a}_f$ ($\hat{a}_f^\dagger$) is the annihilation (creation) operator in the field mode of energy ϵ_f. $\hat{c}^\dagger$ ($\hat{c}$) is the Fermion creation (annihilation) operator belonging to the system (s), left (l), and right (r) leads and ϵ_x is the energy of the x-th mode in the lead. $\hat{V}$ ($\hat{V}^\dagger$) is the system dipole operator which destroys (creates) an excitation in the molecule. T_{sx} is the system−lead tunneling coefficient from the x-th mode of the lead to the s-th orbital of the molecule.

In molecular junctions, the leads create excitations between the many-body states which can radiatively relax and can be detected optically. We are interested in electroluminescence, the optically detected radiative recombination of an electron−hole pair (exciton) created in the same oxidation state. To lowest order, excited states of the ionic charged states, $N \pm 1$, can be created by two molecule−lead interactions that inject an electron or a hole into the molecule. Fluorescence can then arise by a transition between two states belonging to the ionic species (two different oxidation states). We had denoted this process as current induced fluorescence (CIF).[24] Here we focus emission from the same charged state (oxidation state). This requires an injection of an electron and a hole into the molecule and involves four molecule−lead interactions. We call it electroluminescence.

In electroluminescence, formation of an exciton population requires four interactions with the leads which provide several pathways for the evolution of system states that contribute to the signal. We identify all of the possible pathways that populate excitons (electron−hole pair) in the form of two Liouville space loop diagrams[17,19] as shown in Figure 2. These

DOI: 10.1021/acs.jctc.5b00500
J. Chem. Theory Comput. 2015, 11, 4304−4315

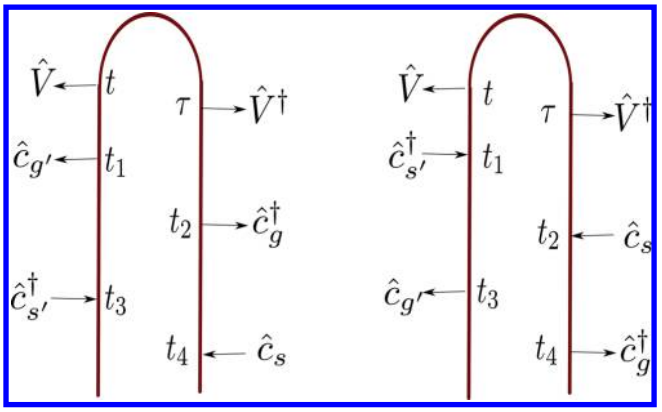

Figure 2. Two Liouville space loops that contribute to electroluminescence caused by populating excitons. Left and right branches are not time-ordered.

diagrams visualize physical processes and allow easy bookkeeping of the various times at which interactions take place. To leading order in molecule–lead interaction, the electroluminescence signal requires a minimum of two interactions from either side of the loop to generate an exciton via populating a charged state. The other diagrams with three (four) interactions from one side and one (no) interaction from the other side give rise to current induced fluorescence and coherent light emission processes. In this work we discard those pathways since we are interested in incoherent spontaneous processes which are the dominant process when the molecule–lead coupling is weak. We follow the standard convention to construct these diagrams. An arrow represents an interaction at a specific time. If it is directed inward (outward) on either branch of the ladder, it represents creation (annihilation) of a new system state with one extra (less) electron in the molecule. The loop is closed via an arc during which there is no evolution. These loops are not time-ordered. One can keep track of the time ordering of the lead interactions and generate several ladder diagrams such that time increases from bottom to top ($t > \tau > t_1 > t_2 > t_3 > t_4$) . The difference between ladder and loop diagrams is that the former is time-ordered whereas the latter is not.

For better understanding, we illustrate the process of electroluminescence by considering one ladder diagram that can be obtained from the loop diagrams and is shown in Figure 3. We label the system orbitals as s,s',g, and g'. The subscripts on the operators provide an identification of the orbital (single particle state) where the operators act. We assume that the system is initially in one of its accessible states with N electrons. We label a Fock state of the molecule with two indices, $|a,N\rangle$ representing the a-th many-body state with N electrons.

In Figure 3, the bra vector (right branch) of the density matrix evolves due to the action of a creation operator at time t_4 due to the molecule–lead coupling Hamiltonian in eq 5. This creates a new many-body state $|b,N+1\rangle$. The state of the system immediately after interaction is $|g,N\rangle\langle b,N+1|$. This represents a Fock space coherence between a neutral and anionic many-body state. Next, the ket (left branch) evolves due to lead interaction at time t_3 leading to a new many-body state, $|c,N+1\rangle\langle b,N+1|$. This represents a coherence in the anionic state. However, if $g = s$, the same state represents a population of the anionic state. Third, during the time evolution $t_3 \rightarrow t_2$, the bra evolves, exciting the system to $|c,N+1\rangle\langle d,N|$, a Fock space coherence. Subsequently at time t_1, the bra evolves such

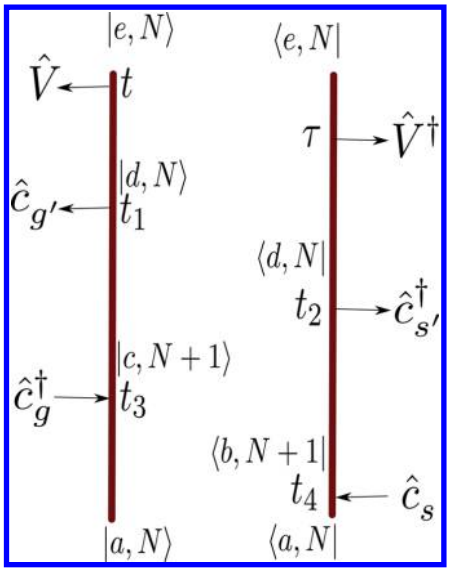

Figure 3. Ladder diagram showing the role of several many-body states during the process of electroluminescence. The interaction times are ordered $t > \tau > t_1 > t_2 > t_3 > t_4$. The four interactions, t_4...t_1 create a single exciton. The excitonic state is $|d,N\rangle\langle d,N|$ which emits a photon of frequency ω_f at time t.

that the system reaches a population state, $|d,N\rangle\langle d,N|$. The state $|d,N\rangle$ contains one exciton. The four interactions at t_4, t_3, t_2, and t_1 create a single exciton in the molecule by evolving the initial state from $|g,N\rangle\langle g,N|$ to $|d,N\rangle\langle d,N|$ via an intermediate charged state. Finally during the evolution $\tau \rightarrow t$, the system relaxes radiatively to state $|e,N\rangle\langle e,N|$, and a signal at frequency ω_f is detected. The final process is represented by interaction with two dipole operators. The entire process involves five time evolutions, t_4 to t_3, t_3 to t_2, t_2 to t_1, t_1 to τ, and τ to t. In order to detect the electroluminescence, it is necessary that the exciton creation takes place before the optical detection: the interaction times t and τ can occur only after the lead interaction times.

III. ELECTROLUMINESCENCE SIGNAL

We use the Liouville space superoperator formalism[19,20,35] to obtain algebraic expressions for the electroluminescence signal. The state of the system is characterized by the density matrix which is a vector denoted as, $|..\rangle\rangle$. The superoperators interacting from left (right) are marked with an index $L(R)$ and are defined as

$$\hat{A}_L|..\rangle\rangle := \hat{A}|.\ \rangle\langle .\ | \qquad \hat{A}_R|..\rangle\rangle := |.\ \rangle\langle .\ |\hat{A} \tag{6}$$

$$\hat{A}_+ = \hat{A}_L + \hat{A}_R \qquad \hat{A}_- = \hat{A}_L - \hat{A}_R \tag{7}$$

$\hat{A}_+$ ($\hat{A}_-$) in the Liouville space corresponds to anticommutation (commutation) in the Hilbert space whose density matrix is written as $|.\rangle\langle .|$. The standard expression for spontaneous optical signal at frequency ω_f is given by ($\hbar = 1$)[19,20,24]

$$S(\omega_f, t) = 2\Re \int_{t_0}^{t} d\tau\ e^{i\omega_f(t-\tau)} \langle\langle \hat{T}\hat{V}_L(t)\ \hat{V}_R^\dagger(\tau)\rangle\rangle \tag{8}$$

$$= 2\Re \int_{t_0}^{t} d\tau\ e^{i\omega_f(t-\tau)} \langle\langle \hat{T}\hat{V}_L(t)\ \hat{V}_R^\dagger(\tau)\ e^{-i\int_{t_0}^{t} d\tau\, \hat{H}_{ml-}(\tau)}\rangle\rangle_o \tag{9}$$

In the second line, we have used the interaction representation defined with respect to the molecule–lead coupling. The time evolution of operators is due to Hamiltonian, $\hat{H}_0$.

DOI: 10.1021/acs.jctc.5b00500
J. Chem. Theory Comput. 2015, 11, 4304–4315

We can now expand eq 9 to fourth order in molecule−lead interaction, $\hat{H}_{ml-}$ (Appendix A). We assume that contributions from coherent processes, where the charged state is never populated (Appendix A), is small as compared to incoherent processes and ignore these pathways. We further neglect the pathways which involve Fock space coherences between many-body states separated by more than one charge units (Appendix A). Such processes contribute with extremely low probability (fast Fock space decoherence). The electroluminescence signal then involves a time-integrated product of a six-point time-dependent system correlation function and a four-point time-dependent lead correlation function given by

$$
\begin{aligned}
S^{el}(\omega_f) = 2\Re \int_{t_0}^{t} \mathrm{d}\tau\ \mathrm{e}^{i\omega_f(t-\tau)} \int_{t_0}^{t} \mathrm{d}t_1 \int_{t_0}^{t} \mathrm{d}t_2 \int_{t_0}^{t} \mathrm{d}t_3 \int_{t_0}^{t} \mathrm{d}t_4 \\
\times \sum_{s,g,s',g'} \sum_{x,x'\in l,r} \sum_{y,y'\in l,r} T^{*}_{s'x'} T_{sx} T^{*}_{g'y'} T_{gy} \\
\times [\langle\langle \hat{T}\hat{c}^{\dagger}_{y'L}(t_1)\ \hat{c}_{yR}(t_2)\ \hat{c}_{x'L}(t_3)\ \hat{c}^{\dagger}_{xR}(t_4)\rangle\rangle_o \\
\times \langle\langle \hat{T}\hat{V}_L(t)\ \hat{V}_R(\tau)\ \hat{c}_{g'L}(t_1)\ \hat{c}^{\dagger}_{gR}(t_2)\ \hat{c}^{\dagger}_{s'L}(t_3)\ \hat{c}_{sR}(t_4)\rangle\rangle_o \\
+ \langle\langle \hat{T}\hat{c}_{x'L}(t_1)\ \hat{c}^{\dagger}_{xR}(t_2)\ \hat{c}^{\dagger}_{y'L}(t_3)\ \hat{c}_{yR}(t_4)\rangle\rangle_o \\
\times \langle\langle \hat{T}\hat{V}_L(t)\ \hat{V}^{\dagger}_R(\tau)\ \hat{c}^{\dagger}_{s'L}(t_1)\ \hat{c}_{sR}(t_2)\ \hat{c}_{g'L}(t_3)\ \hat{c}^{\dagger}_{gR}(t_4)\rangle\rangle_o]
\end{aligned}
\tag{10}
$$

Equation 10 is the basic form of the electroluminescent signal and gives the leading order contribution to the signal at ω_f. Note that eq 10 can directly be read from Figure 2. The first (second) term inside the brackets in eq 10 corresponds to the left (right) loop diagram shown in Figure 2, where $t \geq \tau \geq t_i$, i = 1, ..., 4. Each loop diagram contains four ladder diagrams. All eight ladder diagrams are drawn in Figure 4. It is to be emphasized that both current induced fluorescence (CIF)[24] and electroluminescence are spontaneous processes. However, in CIF the final molecular state differs from the initial state by an electron; i.e., the CIF photon is emitted from a different oxidation state of the molecule than that of the ground state. While in electroluminescence both the initial and the final states have the same number of electrons; i.e., the exciton is formed in the same oxidation state of the molecule as in the ground state, although the pathway involves a change in oxidation state.

The flow of electrons in the junction is maintained by an applied bias and is responsible for the creation of an electron hole pair in the molecule. The applied bias is therefore analogous to the optical laser field in conventional spectroscopy. However, in the present case, the excitations are created by the lead interactions at all energies (summed over x and x' in eq 10). In order to have a signal analogous to the conventional signal, we need to take a derivative of the signal in eq 10 with respect to applied bias. This picks up the contribution due to lead interactions at energy eV. In Appendix B, we present the diagram rules to get closed expressions for the derivative of the signal by directly reading each ladder diagram in Figure (4). The full treatment from which the rules are derived is also discussed in the appendix. These rules apply at low temperatures where there are no thermal fluctuations and the electron flow is effectively unidirectional. The left and right leads are assumed to be the same.

Here we illustrate these rules by applying them to the ladder diagram in Figure 4i. We denote the system many-body states by the letters a, b, c, d, and e. For clarity, we omit the label N which denotes the number of electrons in the state. The system

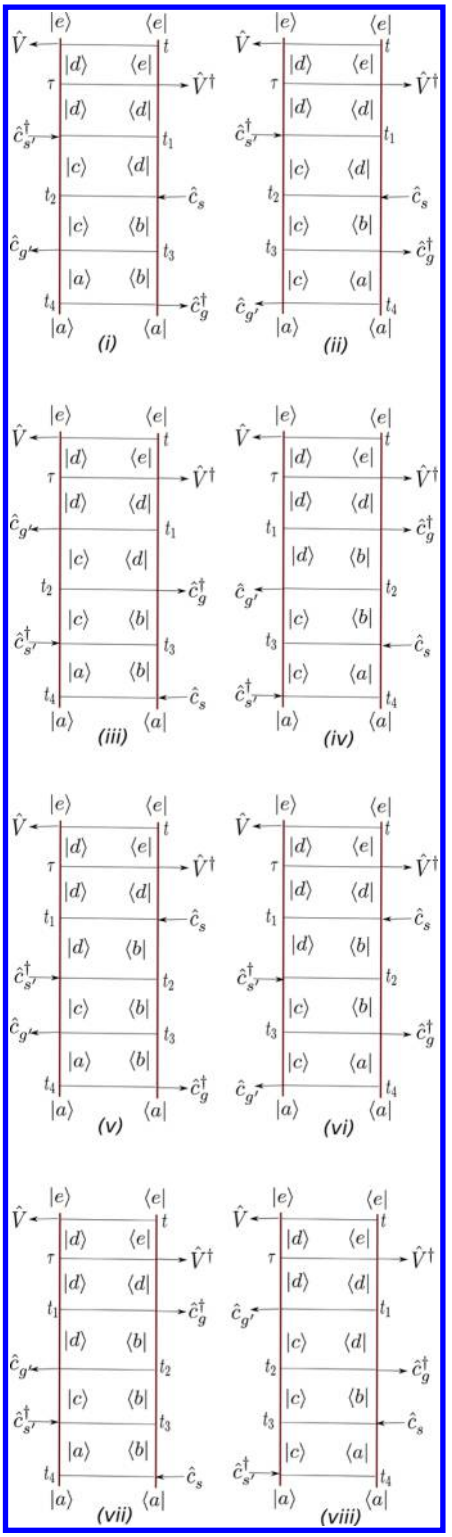

Figure 4. Ladder diagrams showing the contributions to the signal. The various interaction times for each diagram increase from the bottom to the top as t_4, t_3, t_2, t_1, τ, t. t_4 is the first interaction time, and t is the detection time.

starts from ground-state, $\sum_{aa}\rho_{aa}|a\rangle\langle a|$ with probability ρ_{aa}. The initial ground state may correspond to a neutral state or a charged state. Initially, a system operator acts such that the state evolves to $|a\rangle\langle b|$, a coherence between states with a different number of electrons. The corresponding matrix element is $c^{\dagger}_{g,ab}$ (rule 1). Since this is the first interaction pointing outward, the

DOI: 10.1021/acs.jctc.5b00500
J. Chem. Theory Comput. 2015, 11, 4304−4315

Green function during the evolution $t_4 \rightarrow t_3$ does not contribute to the signal (rule 3). At time t_3, another interaction from the left destroys the ket state and the system evolves during $t_3 \rightarrow t_2$ to create Fock space coherence between states with the same number of electrons, $|c\rangle\langle b|$. The corresponding overlap matrix element is read top to bottom as $c_{g',ca}$ The Fock states involved are $|c\rangle$ and $|b\rangle$. $t_3 \rightarrow t_2$ evolution is $\mathcal{G}(\omega_{cb})$ (rule 2). Similarly, the next interaction takes place from the right such that there is a creation in the bra taking the system to the coherent state $|c\rangle\langle d|$ with a different number of electrons. The matrix element is $c_{s,bd}$. Since this interaction is the first inward interaction, the Greens function is $\mathcal{G}(\omega_{cd}+\mathrm{eV})$ (rule 4). The next interaction from the left takes the system to a population state $|d\rangle\langle d|$. The corresponding matrix element and the Greens function are $c^{\dagger}_{s',dc}$ and $\mathcal{G}(\omega_{dd}) = \mathcal{G}(0)$, respectively. Finally, due to interaction with the field, the ket evolves to state $|e\rangle$ from $|d\rangle$ which is the final state. The matrix element is $V^{\dagger}_{ed}$, and the corresponding Greens function is $\mathcal{G}(\omega_{de}-\omega_f)$ (rule 5). The detection interaction contributes via the matrix element V_{de}. Following rule 6, the signal is written as ($\hbar = 1$)

$$\frac{\mathrm{d}}{\mathrm{deV}} S^{((i))}_{el}(\omega_f) = 2\Re \sum_{abcde} \sum_{ss'gg'} \sum_{\nu=l,r} \Omega^2 \rho_{aa} \times T^{\nu}_{s} T^{*\nu}_{s'} T^{\nu'}_{g} T^{*\nu'}_{g'} |V_{de}|^2 c^{\dagger}_{g,ab} c_{g',ca} c_{s,bd} c^{\dagger}_{s',dc} \times \mathcal{G}(0)\, \mathcal{G}(\omega_{de} - \omega_f)\, \mathcal{G}(\omega_{cd} + \mathrm{eV})\, \mathcal{G}(\omega_{cb}) \tag{11}$$

where Ω is the wide-band approximated lead density of states. All of the diagrams can be interpreted in a similar manner. After writing down all of the expressions, we can combine diagram i with ii since their contributions become equal. Similarly we can combine diagram iii with vii, diagram iv with viii, and diagram v with vi. The total electroluminescence signal can now be recast as

$$\begin{aligned}\frac{\mathrm{d}}{\mathrm{deV}} S_{el}(\omega_f) = 4\Re \sum_{abcde} \sum_{ss'gg'} \sum_{\nu=l,r} \Omega^2 \rho_{aa} \times T^{\nu}_{s} T^{*\nu}_{s'} T^{\nu'}_{g} T^{*\nu'}_{g'} |V_{de}|^2\, \mathcal{G}(0)\, \mathcal{G}(\omega_{de} - \omega_f)\, \mathcal{G}(\omega_{cb}) \\ \times [c_{g',ca} c^{\dagger}_{g,ab} c_{s,bd} c^{\dagger}_{s',dc} \mathcal{G}(\omega_{cd} + \mathrm{eV}) \\ + c^{\dagger}_{g',bd} c_{g,dc} c^{\dagger}_{s,ca} c_{s',ab} G(\omega_{ab} + \mathrm{eV}) \\ + c^{\dagger}_{g,bd} c_{g',dc} c_{s,ab} c^{\dagger}_{s',ca} G(\omega_{ca} - \mathrm{eV}) \\ + c^{\dagger}_{g,ab} c_{g',ca} c_{s,bd} c^{\dagger}_{s',dc} G(\omega_{db} - \mathrm{eV})]\end{aligned} \tag{12}$$

Equation 12 is equivalent but a simplified version of eq 10. The time-dependent system and lead correlation functions in eq 10 have been explicitly evaluated and put in closed forms in terms of the system-only Greens functions and the matrix elements of each system operator interacting with a system-only many-body state. We can substitute for the Greens functions as defined in eq B26 and obtain an algebraic expression for the frequency resolved electroluminescence signal given as

$$\begin{aligned}\frac{\mathrm{d}}{\mathrm{deV}} S_{el}(\omega_f) = -4\Im \sum_{abcde} \sum_{ss'gg'} \sum_{\nu=l,r} \Omega^2 \rho_{aa} \\ \times \frac{T^{\nu}_{s} T^{*\nu}_{s'} T^{\nu'}_{g} T^{*\nu'}_{g'} |V_{de}|^2}{\Gamma(\omega_{de} - \omega_f - i\Gamma_{de})(\omega_{cb} - i\Gamma_{cb})} \\ \times \left[\frac{c_{g',ca} c^{\dagger}_{g,ab} c_{s,bd} c^{\dagger}_{s',dc}}{(\omega_{cd} + \mathrm{eV} - i\Gamma_{cd})} + \frac{c^{\dagger}_{g',bd} c_{g,dc} c^{\dagger}_{s,ca} c_{s',ab}}{(\omega_{ab} + \mathrm{eV} - i\Gamma_{ab})} \right. \\ \left. + \frac{c^{\dagger}_{g,bd} c_{g',dc} c_{s,ab} c^{\dagger}_{s',ca}}{(\omega_{ca} - \mathrm{eV} - i\Gamma_{ab})} + \frac{c^{\dagger}_{g,ab} c_{g',ca} c_{s,bd} c^{\dagger}_{s',\mathrm{dc}}}{(\omega_{db} - \mathrm{eV} - i\Gamma_{db})} \right]\end{aligned} \tag{13}$$

Since the signal is expressed in terms of the isolated molecule's Fock states, any quantum chemistry calculation done on the molecule will allow us to identify the system states and the corresponding overlap matrix elements. These can be used to compute the signal. We shall discuss it in more detail in section V.

IV. APPLICATION TO A MULTILEVEL MODEL SYSTEM

We apply the preceding formulation to a three spin−orbital model system coupled to metal leads. We denote the three spin−orbitals by g, s, and s' such that the Fock state can be written as $|lmn\rangle$ where l, m, and n = 0, 1 represent the occupation of each orbital. There are eight many-body states, viz., one state with no electrons ($|000\rangle$), three states with one electron (in any one of the orbitals) ($|100\rangle$, $|010\rangle$, and $|001\rangle$), three states with two orbitals being occupied ($|110\rangle$, $|101\rangle$, and $|011\rangle$), and one triply occupied state (all orbitals are occupied, $|111\rangle$). If one assumes that electron−electron repulsion is very high, all doubly and the triply occupied states can be ignored. This is known as a multilevel Coulomb blockade system. The system thus has only four Fock states available as shown schematically in Figure 5. For simplicity we use $|100\rangle \equiv |1\rangle$, $|010\rangle \equiv |2\rangle$, $|001\rangle \equiv |3\rangle$, and $|000\rangle \equiv |4\rangle$. We assume that the ground state corresponds to one electron state, $|1\rangle$. This can be

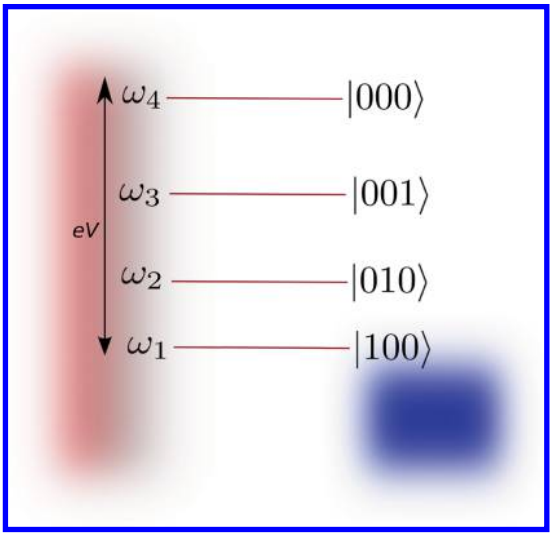

Figure 5. Schematics of the multilevel Coulomb blockade model. $|000\rangle$ is an excited positively charged state. $|100\rangle$ is a ground singlet state; $|010\rangle$ and $|001\rangle$ are two excited singlet states. Electroluminescent photons can be spontaneously emitted from $|010\rangle \rightarrow |100\rangle$, $|001\rangle \rightarrow |100\rangle$, and $|001\rangle \rightarrow |010\rangle$ transition brought about by the dipole operators.

DOI: 10.1021/acs.jctc.5b00500
J. Chem. Theory Comput. 2015, 11, 4304−4315

a situation when the Fermi energy of the leads is between the ground doublet state and the next excited doublet state of the molecule. The next excited state is $|2\rangle$ followed by another excited singlet state $|3\rangle$. $|4\rangle$ represents a cationic state which is the highest in energy.

In this model, the loop diagrams in Figure 2 contribute to the signal only when $g = g'$. Since, the triply occupied state and the doubly occupied states are not accessible, the pathways where the first interaction corresponds to an electron transfer to the molecule do not contribute. Therefore, the first interaction must always create a hole by removing an electron from the molecule. (state $|4\rangle$ is accessible only via removal of an electron from state $|1\rangle$). The diagrams in parts iii, iv, vi, and vii of Figure 4 therefore do not contribute to the electroluminescence in the Coulomb blockade limit. The other four diagrams allow pathways where the hole creation is the first step thereby contributing to the signal and are shown in Figure 6. From

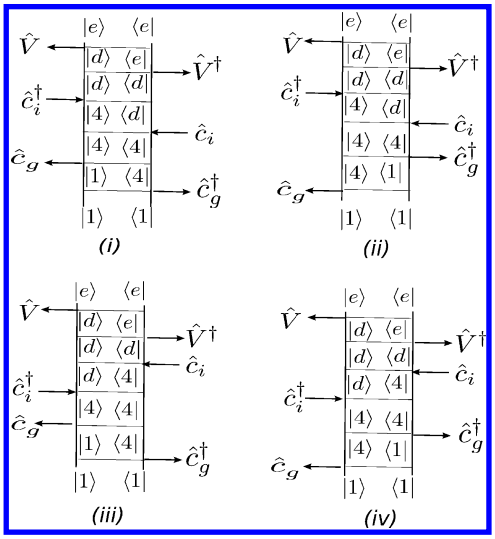

Figure 6. Ladder diagrams for the multilevel Coulomb blockade model. The ground state is marked $|1\rangle \equiv |100\rangle$. $|2\rangle \equiv |010\rangle$, $|3\rangle \equiv |001\rangle$, and $|4\rangle \equiv |000\rangle$. All LSPs involve populating the singly charged state $|4\rangle \equiv |000\rangle$. For $i = s$, the states $|d\rangle = |2\rangle$ and $|e\rangle = |1\rangle$, and for $i = s'$, the states $|d\rangle = |3\rangle$ and $|e\rangle = |2\rangle$ or $|1\rangle$.

Figure 6, we note that the exciton state corresponds to states $|2\rangle$ and $|3\rangle$ (combinedly represented as $|d\rangle$ in the diagram). The radiative relaxation of the state $|2\rangle$ to $|1\rangle$, emits an electroluminescence photon. While the exciton formed at $|3\rangle$ can radiatively relax either to state $|1\rangle$ or state $|2\rangle$. Applying the rules discussed in the previous section and by combining part i with part ii of Figure 6 and part iii with part iv of Figure 6, we get

$$\begin{aligned}\frac{\mathrm{d}}{\mathrm{d}eV}S_{el}(\omega_f) = -4\Re[&|\hat{c}^{\dagger}_{g14}|^2|V_{21}|^2\mathcal{G}(\omega_{44})\,\mathcal{G}(\omega_{22})\,\mathcal{G}(\omega_{21}-\omega_f)\\ &\times\gamma_{sl}\gamma_{gr}\{|\hat{c}_{s42}|^2\mathcal{G}(\omega_{42}+eV)+|\hat{c}^{\dagger}_{s42}|^2\mathcal{G}(\omega_{24}-eV)\}\\ &+\gamma_{s'l}\gamma_{gr}|\hat{c}^{\dagger}_{g14}|^2\mathcal{G}(\omega_{44})\,\mathcal{G}(\omega_{33})\\ &\times\{|V_{31}|^2\mathcal{G}(\omega_{31}-\omega_f)+|V_{32}|^2\mathcal{G}(\omega_{32}-\omega_f)\}\\ &\times\{|\hat{c}_{s'43}|^2\mathcal{G}(\omega_{43}+eV)+|\hat{c}^{\dagger}_{s'43}|^2\mathcal{G}(\omega_{34}-eV)\}]\end{aligned} \tag{14}$$

Here, $\gamma_{jl} = |T^l_j|^2$ is the rate of electron transfer from the left lead to the jth orbital ($j = s, s'$) and $\gamma_{gr} = |T^r_g|^2$ is the rate of electron transfer from the molecule in the g-th orbital to the right lead. Substituting the Greens functions from eq B26, we get

$$\begin{aligned}\frac{\mathrm{d}}{\mathrm{d}eV}S_{el}(\omega_f) = -4\Re\frac{|\hat{c}^{\dagger}_{g14}|^2\gamma_{gr}}{\Gamma_{44}\Gamma_{33}}\Bigg[&\frac{\gamma_{sl}|V_{21}|^2}{(\omega_{21}-\omega_f-i\Gamma_{21})}\\ &\times\left\{\frac{|\hat{c}_{s42}|^2}{\omega_{42}+eV-i\Gamma_{42}}+\frac{|\hat{c}^{\dagger}_{s42}|^2}{\omega_{24}-eV-i\Gamma_{24}}\right\}\\ &+\left\{\frac{\gamma_{s'l}|V_{31}|^2}{\omega_{31}-\omega_f-i\Gamma_{31}}+\frac{\gamma_{s'l}|V_{32}|^2}{\omega_{32}-\omega_f-i\Gamma_{32}}\right\}\\ &\times\left\{\frac{|\hat{c}_{s'43}|^2}{\omega_{43}+eV-i\Gamma_{43}}+\frac{|\hat{c}^{\dagger}_{s'43}|^2}{\omega_{34}-eV-i\Gamma_{34}}\right\}\Bigg]\end{aligned} \tag{15}$$

Here Γ_{ij} is the inverse lifetime of the $i \to j$ transition and Γ_{ii} is the total inverse lifetime of the ith state. We see a total of three peaks, viz., $|2\rangle \to |1\rangle$, $|3\rangle \to |1\rangle$, and $|3\rangle \to |2\rangle$. Since the molecule is initially in state $|1\rangle$, it loses an electron and excites itself to the cationic state $|4\rangle$. From $|4\rangle$ there are only two excited states $|2\rangle$ and $|3\rangle$ that it can access through electron transfer. Therefore, the evolution to these two excited states depend on the applied bias. The first term in eq 15 corresponds to the transition $|2\rangle \to |1\rangle$, while the second term is a combination of the $|3\rangle \to |1\rangle$ and the $|3\rangle \to |2\rangle$ transitions.

The maximum intensity of the signal corresponds to the resonance. As we move off-resonance, the peak intensity decreases gradually due to the broadening quantified by the inverse lifetime as shown in Figure (7). In this case there exists

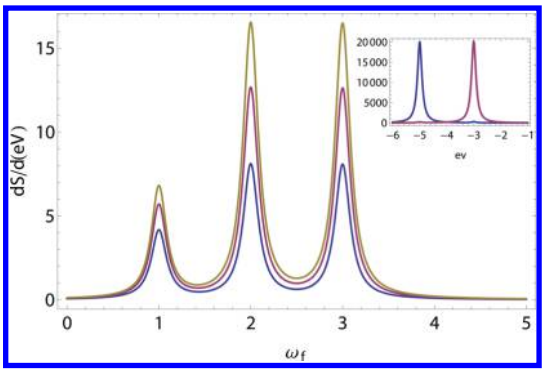

Figure 7. Electroluminescence spectrum (arbitrary units) of the multilevel Coulomb blockade model signal vs detected frequency simulated at various applied bias values. All couplings and matrix elements are set to unity. All lifetimes are set to 0.1, and $\omega_1 = 0$, $\omega_2 = 1$, $\omega_3 = 3$, and $\omega_4 = 6$. From top to bottom, curves correspond to eV = 0.5, 1, and 2, respectively. The three maxima in the intensity correspond to the resonances $\omega_f = \omega_{21} = 1$, $\omega_{32} = 2$, and $\omega_{31} = 3$. The inset shows the nonlinear dependence of the signal intensity on the applied bias. The left (right) peak curve is for the transition $|2\rangle \to |1\rangle$ ($|3\rangle \to |2\rangle$). The spectrum is evaluated at resonance.

another resonance; when the applied bias equals the excitation energy difference as can be seen from eq 15. E.g., for the electroluminescent transition $|3\rangle \to |2\rangle$, the overall maximum intensity is when both of the resonances take place; i.e., $\omega_{32} = \omega_f$ and $\omega_{43} = -eV$. This is expected since the only way to populate state $|3\rangle$ is via $|4\rangle$, and when the bias energy is in resonance with ω_{43}, this process is most probable as seen in Figure 8 and the inset of Figure 7. In the inset of Figure 7, we

DOI: 10.1021/acs.jctc.5b00500
J. Chem. Theory Comput. 2015, 11, 4304−4315

plot the transitions $|2\rangle \rightarrow |1\rangle$ and $|3\rangle \rightarrow |2\rangle$ at their resonance values ($\omega_{21} = \omega_f$, $\omega_{32} = \omega_f$) as a function of bias.

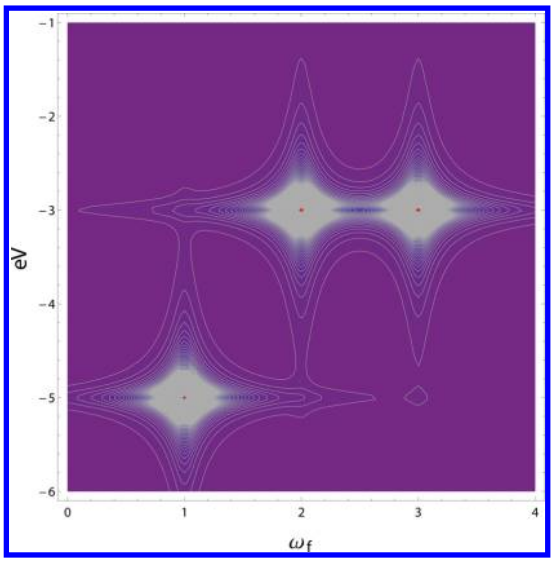

Figure 8. Electroluminescence spectrum in the multilevel Coulomb blockade system vs the bias voltage vs all emitted frequency ω_f. The bottom left maximum is at the resonance of $\omega_{21} = \omega_f$ and $\omega_{42} = -$eV. The middle maximum is at the resonance $\omega_{32} = \omega_f$ and $\omega_{43} = -$eV. The bottom-right peak corresponds to $\omega_{31} = \omega_f$ and $\omega_{43} = -$eV.

Note that, the electroluminescence is not possible if the ground state of the Coulomb blockade model system is in the cationic state, $|4\rangle$. This is because there is no other cationic excited many-body state from which a radiative relaxation to state $|4\rangle$ can take place. For electroluminescent emission of a photon, we need at least two many-body states which have the same oxidation state and a many-body state that differs by one oxidation number.

V. APPLICATION TO GOLD−BENZENE-1,4-DITHIOL−GOLD MOLECULAR JUNCTION

We now consider a single benzene-1,4-dithiol molecule which is connected to two gold leads. This molecular junction is widely studied and is similar to break-junctions.[36] We take the optimized geometry and quantum chemistry parameters, including energies, transition dipole moments (TDMs), and generalized overlap amplitudes (GOAs), from our previous work.[37] In our simulation we choose three Au-atoms bonded to each of the sulfurs as shown in Figure 9. The internuclear distance between the two Au atoms is fixed at 2.88 Å, taken from the distance in the Au(111) surface.[38] In the optimized geometry, the distance between S and the Au(111) surface is around 2.3 Å. Ten excited states were calculated at the time-dependent DFT level with the Tamm−Dancoff approximation[39] by using a locally modified NWChem package.[40,41] After filtering out nonphysical states with large spin contaminations, 10, 7, and 5 excited states for the neutral, cationic (n−1), and anionic (n+1) molecule were obtained. The anionic molecule has the lowest ground state energy. We rescale all of the other many-body energies relative to this state (labeled as $|g_0\rangle$) which is taken as zero. The 5 excited states for the anion are labeled as $|g_i\rangle$, i = 1, ..., 5. Similarly, the ground and 10 excited states of the neutral molecule are labeled as $|e_i\rangle$, i = 0, ..., 10. The cationic states lie very high in energy (>9 eV) in comparison to the

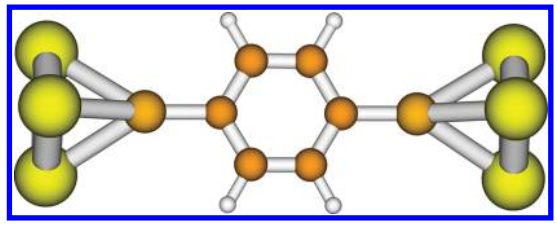

Figure 9. Gold−benzene-1,4-dithiol−gold molecular junction. The yellow balls represent Au atoms. The bigger brown balls connected to Au are S atoms. The small brown and gray balls, respectively, represent carbon and hydrogen atoms. The Au atoms represent the Au (111) surface, and the S atom sits in its hollow site. The left Au lead is at chemical potential eV and acts as the source of electrons which flow through the junction. The chemical potential of the right Au lead is 0 and acts as an electron sink.

neutral and anionic states. Within our bias range of 0−5 eV, these cationic states cannot be populated. So we restrict our calculations to only the neutral and the anionic many-body states. The only dipole allowed transitions are between the states with the same number of electrons. Dipole excitations between excited many-body states are neglected. The energies and the x-component of the transition dipole matrix elements (TDMEs) are given in Table 1.

Table 1. Parameters Used for Calculation

many-body state	ω_m (eV)	TDME
$\|g_o\rangle$	0.0000	$\langle g_o\|V\|g_o\rangle$ = 0.0000
$\|g_1\rangle$	0.1339	$\langle g_o\|V\|g_1\rangle$ = 0.0099
$\|g_2\rangle$	0.1602	$\langle g_o\|V\|g_2\rangle$ = 0.6354
$\|g_3\rangle$	0.8549	$\langle g_o\|V\|g_3\rangle$ = 4.6131
$\|g_4\rangle$	1.2397	$\langle g_o\|V\|g_4\rangle$ = 0.1970
$\|g_5\rangle$	1.2596	$\langle g_o\|V\|g_5\rangle$ = 0.0026
$\|e_o\rangle$	2.7950	$\langle e_o\|V\|e_o\rangle$ = 0.0000
$\|e_1\rangle$	4.1422	$\langle e_o\|V\|e_1\rangle$ = 0.2098
$\|e_2\rangle$	4.1628	$\langle e_o\|V\|e_2\rangle$ = 0.0037
$\|e_3\rangle$	4.4538	$\langle e_o\|V\|e_3\rangle$ = 3.3120
$\|e_4\rangle$	4.6019	$\langle e_o\|V\|e_4\rangle$ = 0.1227
$\|e_5\rangle$	4.7224	$\langle e_o\|V\|e_5\rangle$ = 0.0122
$\|e_6\rangle$	4.7684	$\langle e_o\|V\|e_6\rangle$ = 0.0096
$\|e_7\rangle$	5.0353	$\langle e_o\|V\|e_7\rangle$ = 0.3512
$\|e_8\rangle$	5.1160	$\langle e_o\|V\|e_8\rangle$ = 1.2642
$\|e_9\rangle$	5.1613	$\langle e_o\|V\|e_9\rangle$ = 0.0080
$\|e_{10}\rangle$	5.1823	$\langle e_o\|V\|e_{10}\rangle$ = 0.2363

At finite bias, electrons start to flow through the molecular junction and electroluminescence may be observed. We compute the signal using eq 13 as a function of detected frequency ω_f at different eV values. The summations over the many-body states in eq 13 run over all of the 17 many-body states. The inverse lifetimes are directly proportional to the width of the signal. Although it is possible to obtain the lifetime from fluorescence measurements, we treat these as parameters in our simulation. We fix $\Gamma = 0.01$, $\Gamma_{de} = 0.005$, $\Gamma_{cb} = 0.01$, and $\Gamma_{cd} = \Gamma_{ab} = \Gamma_{ca} = \Gamma_{db} = 0.001$. All energies are given in eV. Plugging the respective values for the matrix elements and energies from Table 1 and constructing the GOAs, the signal can be numerically evaluated. Since the ground state corresponds to the anionic (N+1) state, the emission of the electroluminescent photon comes from the anionic many-body state. We expect a total of five peaks in the signal emitted from the excited anionic many-body states. However, the transition

DOI: 10.1021/acs.jctc.5b00500
J. Chem. Theory Comput. 2015, 11, 4304−4315

dipole matrix elements $\langle g_o|V|g_1\rangle$ and $\langle g_o|V|g_5\rangle$ are very small as compared to the other elements. This renders both transitions too weak to be detected. As a result we see only three peaks as shown in Figure 10. The dipole coupling $\langle g_o|V|g_3\rangle$ is the highest and hence the transition is the strongest of the three.

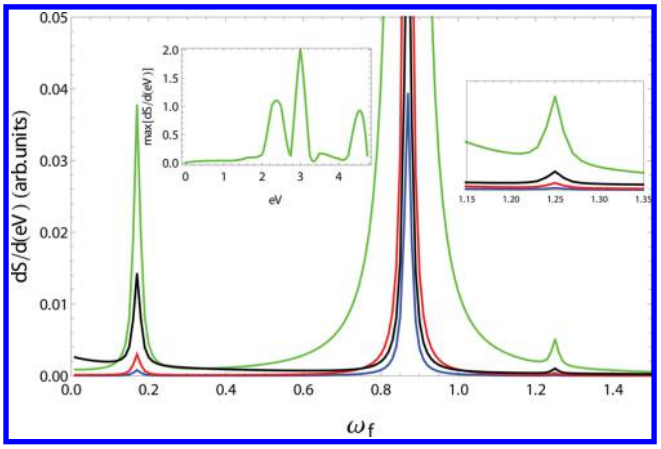

Figure 10. Electroluminescent spectrum of the gold−benzene-1,4-dithiol−gold molecular junction. The various curves correspond to different bias values. From the the highest intensity peak (green), the bias (in eV) values are 3, 4, 2, and 1. Top right inset shows the expanded spectrum at ω_f corresponding to the transition $|g_4\rangle \rightarrow |g_o\rangle$. The left inset shows the intensity variation of the signal with bias at frequency ω_f corresponding to the transition $|g_3\rangle \rightarrow |g_o\rangle$ (central peak).

In Figure 10, the left peak corresponds to the transition $|g_2\rangle \rightarrow |g_o\rangle$, the middle peak to the transition $|g_3\rangle \rightarrow |g_o\rangle$, and the weak right peak, which is also shown in the expanded top-right inset, to the transition $|g_4\rangle \rightarrow |g_o\rangle$. The left inset shows the variation in the signal intensity at ω_f corresponding to the transition $|g_3\rangle \rightarrow |g_o\rangle$ as a function of the bias. The intensity variation shows a nonlinear bias dependence. The presence of multiple maxima as a function of bias is due to the multiple transitions in the junction which resonate with the bias at different values.

VI. CONCLUSIONS

We have presented a Liouville space diagrammatic method for calculating the electroluminescence signal in a molecular junction. The various Liouville space pathways through which the signal can be generated are identified. We considered only the incoherent pathways which involve populating the charged (anionic or cationic) states of the molecule. Although the presented diagrammatic approach is valid for all pathways, for clarity, we have ignored the coherent contributions which are assumed to be small in the weak molecule−lead coupling limit. Two loop diagrams can be drawn from which eight time-ordered incoherent ladder diagrams leading to electroluminescence can be constructed. We discussed signals in terms of the derivative with respect to the applied bias. Diagram rules allow one to read the algebraic form of the signals directly from the diagrams. The method is applied to compute the electroluminescent signal from a multilevel Coulomb blockade model system and a molecular junction made of benzene-1,4-dithiol molecule coupled to two Au leads.

APPENDIX

Appendix A: Microscopic Formulation of Electroluminescence

The signal is defined as the rate of change of photon occupation in the detected mode

$$S(t) = \frac{\mathrm{d}}{\mathrm{d}t}\langle\langle \hat{a}_f^\dagger(t)\, \hat{a}_f(t)\rangle\rangle_F \tag{A1}$$

Here the subscript f represents the detected field mode and the trace is over the full (molecule + field + leads) density matrix denoted as a subscript F. Using the Heisenberg's equation of motion in eq A1 and the definition of coupling Hamiltonian from eq 5, we can express the full signal in terms of Liouville space superoperators as ($\hbar = 1$)

$$S(t) = -2\Im\langle\langle \hat{\mathcal{E}}_{fL}(t)\, \hat{V}_L^\dagger(t)\rangle\rangle_F \tag{A2}$$

Defining the interaction picture with respect to molecule−field coupling, we get

$$\hat{\mathcal{E}}_{fL}^\dagger(t) = \mathrm{e}^{i\hat{H}_f t}\hat{\mathcal{E}}_{fL}^\dagger \mathrm{e}^{-i\hat{H}_f t} \tag{A3}$$

$$\hat{V}_L(t) = \mathrm{e}^{i(\hat{H}_{m-}+\hat{H}_{ml-})t}\hat{V}_L \mathrm{e}^{-i(\hat{H}_{m-}+\hat{H}_{ml-})t} \tag{A4}$$

such that

$$S(t) = -2\Im\langle\langle \hat{\mathcal{T}}\hat{\mathcal{E}}_{fL}(t)\, \hat{V}_L^\dagger(t)\, \mathrm{e}^{-i\int_{t_0}^t \mathrm{d}\tau\, \hat{H}_{mf-}(\tau)}\rangle\rangle \tag{A5}$$

Here, $\hat{H}_-(\tau) = \hat{H}_L(\tau) - \hat{H}_R(\tau)$ and $\hat{\mathcal{T}}$ is the Liouville space time ordering operator.[17] The trace in eq A5 is over the product of the field and the interacting molecule−lead density matrix. The evolution of this density matrix is due to molecule−field interaction. eq A5 contains both the spontaneous and the stimulated light emission processes. To leading order in the detected field (molecule−field interaction, $\hat{H}_{mf-}$), we can recast the signal as

$$S(t) = -2\Re\{\int_{t_0}^t \mathrm{d}\tau\, \langle\langle \hat{\mathcal{T}}\hat{\mathcal{E}}_{fL}^\dagger(t)\, \hat{\mathcal{E}}_{fL}(\tau)\rangle\rangle_o \langle\langle \hat{\mathcal{T}}\hat{V}_L(t)^\dagger\, \hat{V}_L(\tau)\rangle\rangle - \langle\langle \hat{\mathcal{T}}\hat{\mathcal{E}}_{fR}(t)\, \hat{\mathcal{E}}_{fL}^\dagger(\tau)\rangle\rangle_o \langle\langle \hat{\mathcal{T}}\hat{V}_L(t)\, \hat{V}_R^\dagger(\tau)\rangle\rangle\} \tag{A6}$$

The subscript o identifies that the trace is over the bare density matrix of individual system components. Since we are interested in the spontaneous signal, we assume that the detected mode is initially empty. Setting $|E_f|^2 = 1$, we can arrive at eq 8.

We now evaluate eq 10. Starting from eq 9, we define the interaction picture with respect to molecule−lead interaction as

$$\hat{V}_L(t) = \mathrm{e}^{i\hat{H}_{m-}t}\hat{V}_L \mathrm{e}^{-i\hat{H}_{m-}t} \tag{A7}$$

$$\hat{V}_R(t) = \mathrm{e}^{-i\hat{H}_{m-}t}\hat{V}_R \mathrm{e}^{i\hat{H}_{m-}t} \tag{A8}$$

The subscript o identifies that the trace is over the bare density matrix of individual system components. In this representation the trace of the correlation function in the RHS of eq 9 is with respect to the bare molecular density matrix which evolves due to molecule−lead interaction. We expand eq 9 to fourth order (lowest contributing) in the molecule−lead coupling, H_{ml-}. The RHS in eq 9 can be now written as

$$= \int_{t_0}^t \mathrm{d}t_1 \int_{t_0}^t \mathrm{d}t_2 \int_{t_0}^t \mathrm{d}t_3 \int_{t_0}^t \mathrm{d}t_4\, \langle\langle \mathcal{T}\hat{V}_L(t)\, \hat{V}_R^\dagger(\tau) \times \hat{H}_{ml-}(t_1)\, \hat{H}_{ml-}(t_2)\, \hat{H}_{ml-}(t_3)\, \hat{H}_{ml-}(t_4)\rangle\rangle_o \tag{A9}$$

DOI: 10.1021/acs.jctc.5b00500
J. Chem. Theory Comput. 2015, 11, 4304−4315

The time arguments get integrated since they are not controlled externally. Upon substituting $\hat{H}_{ml-} = \hat{H}_{mlL} - \hat{H}_{mlR}$, we get 16 terms in the equation. Out of the 16 terms only the terms with two *L*s and two *R*s in the lead operators contribute to electroluminescence. The other terms contribute to current induced fluorescent signals which may come from either the neutral or the charged states. The electroluminescent signal can be expressed as

$$\begin{aligned} S^{el}(\omega_f, t) = 2\Re\mathcal{T}\int_{t_0}^{t} d\tau\, e^{i\omega_f(t-\tau)}\int_{t_o}^{t} dt_1\int_{t_0}^{t} dt_2\int_{t_0}^{t} dt_3\int_{t_0}^{t} dt_4 \\ \times(\langle\langle\hat{V}_L(t)\,\hat{V}_R^{\dagger}(\tau)\,\hat{H}_{mlL}(t_1)\,\hat{H}_{mlL}(t_2)\,\hat{H}_{mlR}(t_3)\,\hat{H}_{mlR}(t_4)\rangle\rangle_o \\ + \langle\langle V_L(t)\,V_R^{\dagger}(\tau)\,\hat{H}_{mlL}(t_1)\,\hat{H}_{mlR}(t_2)\,\hat{H}_{mlL}(t_3)\,\hat{H}_{mlR}(t_4)\rangle\rangle_o \\ + \langle\langle\hat{V}_L(t)\,\hat{V}_R^{\dagger}(\tau)\,\hat{H}_{mlL}(t_1)\,\hat{H}_{mlR}(t_2)\,\hat{H}_{mlR}(t_3)\,\hat{H}_{mlL}(t_4)\rangle\rangle_o \\ + \langle\langle\hat{V}_L(t)\,\hat{V}_R^{\dagger}(\tau)\,\hat{H}_{mlR}(t_1)\,\hat{H}_{mlL}(t_2)\,\hat{H}_{mlL}(t_3)\,\hat{H}_{mlR}(t_4)\rangle\rangle_o \\ + \langle\langle\hat{V}_L(t)\,V_R^{\dagger}(\tau)\,\hat{H}_{mlR}(t_1)\,\hat{H}_{mlL}(t_2)\,\hat{H}_{mlR}(t_3)\,\hat{H}_{mlL}(t_4)\rangle\rangle_o \\ + \langle\langle\hat{V}_L(t)\,V_R^{\dagger}(\tau)\,\hat{H}_{mlR}(t_1)\,\hat{H}_{mlR}(t_2)\,\hat{H}_{mlL}(t_3)\,\hat{H}_{mlL}(t_4)\rangle\rangle_o) \end{aligned} \tag{A10}$$

For weak system bath coupling, the perturbation formulation allows us to factorize the system and lead correlation functions after substituting the molecule−lead coupling Hamiltonian from eq 5 in eq A10. The system correlation function includes the product of all of the system operators along with their time arguments in the loop diagrams. The product is averaged over the system density matrix, $|\rho\rangle\rangle$. For each system operator there is a corresponding lead operator. Since creation of electron in the system is annihilation of an electron in the lead, the lead operators are conjugate to each of the system operators. The dipole operators have no lead counterpart.

In the first term of eq A10, one of the system correlation functions is $\langle\langle\hat{V}_L(t)\ \hat{V}_R(\tau)\ \hat{c}_{g'L}(t_1)\ \hat{c}_{gL}^{\dagger}(t_2)\ \hat{c}_{s'R}^{\dagger}(t_3)\ \hat{c}_{sR}(t_4)\rangle\rangle_o$, Figure 11i. The first interaction destroys a system electron in the bra. The second interaction creates a system electron in the ket. The molecule is now in a Fock space coherent state with the same number of electrons. The next two interactions from the right excite the system to some other Fock space coherent state with the same number of electrons. This state emits a photon. This is a higher order spontaneous light emission process from a neutral state in which the system evolved through coherences alone. We identify such processes as coherence induced luminescence, and they are different from current induced fluorescence or electroluminescence.

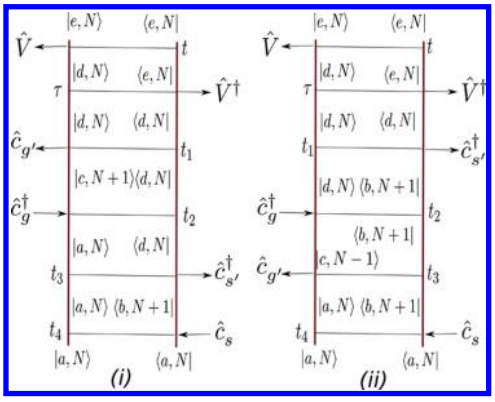

Figure 11. Ladder diagrams involving (i) coherence induced luminescence and (ii) higher order Fock space coherence. In i, the pathway does not populate a charged state and evolves coherently throughout. In ii, during the time evolution $t_3 \rightarrow t_2$, the state of the system is $|c,N-1\rangle\langle b,N+1|$. This higher order Fock space coherence occurs with extremely low probability. These pathways are ignored in the present calculations.

Another system correlation function is of the type $\langle\langle\hat{V}_L(t)\ \hat{V}_R(\tau)\ \hat{c}_{sR}(t_1)\ \hat{c}_{g'L}(t_2)\ \hat{c}_{gL}^{\dagger}(t_3)\ \hat{c}_{s'R}(t_4)\rangle\rangle_o$, Figure 11ii. The first two interactions are from the right and hence create two consecutive electrons in the bra. The next interaction is from the left and creates an electron in the ket. This generates a higher order Fock space coherence between states which differ by more than one electron. These coherences are very fast and occur with very low probability. So, we neglect such correlation functions. We finally have two terms left in eq A10, which is equivalent to eq 10 and corresponds to the two loop diagrams shown in Figure 2.

Appendix B: Evaluation of Equation 13

Expanding the time-ordered integrals in eq 10, we get eight expressions which correspond to the eight ladder diagrams shown in Figure 4. Writing down the time evolution explicitly, the signal becomes

$$\begin{aligned} S^{el}(\omega_f, t) = 2\Re\int_{t_0}^{t} d\tau\, e^{i\omega_f(t-\tau)}\sum_{ss'gg'}\sum_{x,y} T_{s'x}T_{sx'}^{*}T_{gy'}T_{g'y}^{*} \\ \times\int_{t_o}^{\tau} dt_1\int_{t_0}^{t_1} dt_2\int_{t_0}^{t_2} dt_3\int_{t_0}^{t_3} dt_4\sum_i S_i \end{aligned} \tag{B1}$$

where S_i corresponds to the *i*th ladder diagram (Figure 4) given as

$$S_1 = \langle\langle\hat{V}_L(t)\,\hat{V}_R^{\dagger}(\tau)\,\hat{c}_{s'L}^{\dagger}(t_1)\,\hat{c}_{sR}(t_2)\,\hat{c}_{g'L}(t_3)\,\hat{c}_{gR}^{\dagger}(t_4)\rangle\rangle_o \times\langle\langle\hat{c}_{xL}\hat{c}_{x'R}^{\dagger}\hat{c}_{yL}\hat{c}_{y'R}^{\dagger}\rangle\rangle_o e^{i(\omega_x t_1-\omega_{x'}t_2-\omega_y t_3+\omega_{y'}t_4)} \tag{B2}$$

$$S_2 = \langle\langle\hat{V}_L(t)\,\hat{V}_R^{\dagger}(\tau)\,\hat{c}_{s'L}^{\dagger}(t_1)\,\hat{c}_{sR}(t_2)\,\hat{c}_{gR}^{\dagger}(t_3)\,\hat{c}_{g'L}(t_4)\rangle\rangle_o \times\langle\langle\hat{c}_{xL}\hat{c}_{xR}^{\dagger}\hat{c}_{yR}\hat{c}_{yL}^{\dagger}\rangle\rangle_o e^{i(\omega_x t_1-\omega_{x'}t_2+\omega_y t_3-\omega_{y'}t_4)} \tag{B3}$$

$$S_3 = \langle\langle\hat{V}_L(t)\,\hat{V}_R^{\dagger}(\tau)\,\hat{c}_{gL}(t_1)\,\hat{c}_{g'R}^{\dagger}(t_2)\,\hat{c}_{sL}^{\dagger}(t_3)\,\hat{c}_{s'L}(t_4)\rangle\rangle_o \times\langle\langle\hat{c}_{yL}^{\dagger}\hat{c}_{yR}\hat{c}_{xL}\hat{c}_{xL}^{\dagger}\rangle\rangle_o e^{i(\omega_y t_1-\omega_{y'}t_2-\omega_x t_3+\omega_{x'}t_4)} \tag{B4}$$

$$S_4 = \langle\langle\hat{V}_L(t)\,\hat{V}_R^{\dagger}(\tau)\,\hat{c}_{gR}^{\dagger}(t_1)\,\hat{c}_{g'L}(t_2)\,\hat{c}_{sR}(t_3)\,\hat{c}_{s'L}^{\dagger}(t_4)\rangle\rangle_o \times\langle\langle\hat{c}_{yR}\hat{c}_{yL}^{\dagger}\hat{c}_{xR}^{\dagger}\hat{c}_{xL}\rangle\rangle_o e^{i(-\omega_y t_1+\omega_{y'}t_2+\omega_x t_3-\omega_{x'}t_4)} \tag{B5}$$

$$S_5 = \langle\langle\hat{V}_L(t)\,\hat{V}_R^{\dagger}(\tau)\,\hat{c}_{sR}(t_1)\,\hat{c}_{s'L}^{\dagger}(t_2)\,\hat{c}_{g'L}(t_3)\,\hat{c}_{gR}^{\dagger}(t_4)\rangle\rangle_o \times\langle\langle\hat{c}_{yR}\hat{c}_{yL}^{\dagger}\hat{c}_{xR}^{\dagger}\hat{c}_{xL}\rangle\rangle_o e^{i(\omega_x t_1-\omega_{x'}t_2+\omega_y t_3-\omega_{y'}t_4)} \tag{B6}$$

$$S_6 = \langle\langle\hat{V}_L(t)\,\hat{V}_R^{\dagger}(\tau)\,\hat{c}_{sR}(t_1)\,\hat{c}_{s'L}^{\dagger}(t_2)\,\hat{c}_{gR}^{\dagger}(t_3)\,\hat{c}_{g'L}(t_4)\rangle\rangle_o \times\langle\langle\hat{c}_{yR}\hat{c}_{yL}^{\dagger}\hat{c}_{xR}\hat{c}_{xL}^{\dagger}\rangle\rangle_o e^{i(\omega_x t_1--\omega_{x'}t_2-\omega_y t_3+\omega_{y'}t_4)} \tag{B7}$$

$$S_7 = \langle\langle V_L(t)\,V_R^{\dagger}(\tau)\,c_{gR}^{\dagger}(t_1)\,c_{g'L}(t_2)c_{s'L}^{\dagger}(t_3)\,c_{sL}(t_4)\rangle\rangle_o \times\langle\langle\hat{c}_{yR}\hat{c}_{yL}^{\dagger}\hat{c}_{xR}\hat{c}_{xL}^{\dagger}\rangle\rangle_o e^{i(-\omega_y t_1+\omega_{y'}t_2-\omega_x t_3+\omega_{x'}t_4)} \tag{B8}$$

$$S_8 = \langle\langle\hat{V}_L(t)\,\hat{V}_R^{\dagger}(\tau)\,\hat{c}_{g'L}(t_1)\,\hat{c}_{gR}^{\dagger}(t_2)\,\hat{c}_{sL}(t_3)\,\hat{c}_{s'L}^{\dagger}(t_4)\rangle\rangle_o \times\langle\langle\hat{c}_{yR}\hat{c}_{yL}^{\dagger}\hat{c}_{xR}\hat{c}_{xL}^{\dagger}\rangle\rangle_o e^{i(\omega_y t_1-\omega_{y'}t_2+\omega_x t_3-\omega_{x'}t_4)} \tag{B9}$$

For clarity, we first consider the evaluation of expression S_1. We denote the ground state to be $\sum_a \rho_{aa}|a\rangle\langle a|$ (ρ_{aa} is the initial

DOI: 10.1021/acs.jctc.5b00500
J. Chem. Theory Comput. 2015, 11, 4304−4315

probability) and insert the identity $I = \sum_n |n\rangle\langle n|$, in terms of molecular many-body states $|n\rangle$. Using the mapping between Liouville space and Hilbert space,[35] we have

$$\hat{c}_{iL}|\rho\rangle\rangle \equiv \hat{c}_i\rho \tag{B10}$$

$$\hat{c}^{\dagger}_{iL}|\rho\rangle\rangle \equiv \hat{c}^{\dagger}_i\rho \tag{B11}$$

$$\hat{c}_{iR}|\rho\rangle\rangle \equiv (-1)^{M-N}\rho\hat{c}_i \tag{B12}$$

$$\hat{c}^{\dagger}_{iR}|\rho\rangle\rangle \equiv (-1)^{M-N+1}\rho\hat{c}^{\dagger}_i \tag{B13}$$

where $\rho = \sum|M\rangle\langle N|$ is the Hilbert space density matrix. The system-only correlation function in S_1 can be recast into the Hilbert space operators.

$$\begin{aligned}\langle\langle \hat{V}_L(t)\ \hat{V}^{\dagger}_R(\tau)\ \hat{c}^{\dagger}_{s'L}(t_1)\ \hat{c}_{sR}(t_2)\ \hat{c}_{g'L}(t_3)\ \hat{c}^{\dagger}_{gR}(t_4)\rangle\rangle_o \\ = \sum_{abcde} \rho_{aa}\,|V_{de}|^2\, c^{\dagger}_{g,ab}c_{g',ca}c_{s,bd}c^{\dagger}_{s',dc} \\ \times\, e^{i(\omega_{ab}t_4+\omega_{bc}t_3+\omega_{dc}t_2+\omega_{de}t_1-(\omega_f+\omega_{ed})(t-\tau))}\end{aligned} \tag{B14}$$

where we denoted the matrix element, $A_{k,nn'} = \langle n|A_k|n'\rangle$.

The lead correlation function in S_1 can be recast into the Hilbert space as $\langle\langle \hat{c}_{xL}\hat{c}_{x'R}\hat{c}^{\dagger}_{yL}\hat{c}_{y'R}\rangle\rangle_o = \langle \hat{c}_{y'}\hat{c}^{\dagger}_x\hat{c}_x\hat{c}^{\dagger}_y\rangle$. Since the two leads do not interact among themselves one can separate the four point correlation function as a product of two separate two point correlation functions, $\langle \hat{c}_{y'}\hat{c}^{\dagger}_x\hat{c}_x\hat{c}^{\dagger}_y\rangle = \langle \hat{c}_{y'}\hat{c}^{\dagger}_y\rangle\langle \hat{c}^{\dagger}_x\hat{c}_x\rangle + \langle \hat{c}_x\hat{c}^{\dagger}_x\rangle\langle \hat{c}^{\dagger}_y\hat{c}_{y'}\rangle + \langle \hat{c}_{y'}\hat{c}^{\dagger}_x\rangle\langle \hat{c}^{\dagger}_y\hat{c}_y\rangle + \langle \hat{c}_x\hat{c}^{\dagger}_x\rangle\langle \hat{c}^{\dagger}_y\hat{c}_{y'}\rangle$. So, $\langle \hat{c}^{\dagger}_x\hat{c}_x\rangle = f_x$ and $\langle \hat{c}_x\hat{c}^{\dagger}_x\rangle = 1 - f_x = \bar{f}_x$, where f_x's are the Fermi functions of the lead at the energy ω_x such that $x \in l, r$ defined as $f_x = 1/(e^{(\hbar\omega_x-\mu_x)/kT_x} + 1)$ and μ_x is the chemical potential of the xth lead which are at temperatures T_x. The contribution from S_1 to the signal after simplification can be written down as

$$\begin{aligned}S^{el}_1(\omega_f, t) = 2\Re \sum_{ss'gg'}\sum_{xy}\sum_{abcde} T^x_{s'}T^{x*}_s T^y_g T^{y*}_{g'}\rho_{aa}|V_{de}|^2 \\ \times\, c^{\dagger}_{g,ab}c_{g',ca}c_{s,bd}c^{\dagger}_{s',dc}(f_x\tilde{f}_y + f_y\tilde{f}_x + f_x\bar{f}_x + f_y\bar{f}_y) \\ \times \int_{t_0}^{t} d\tau\, e^{i\omega_f(t-\tau)}\int_{t_0}^{\tau} dt_1\int_{t_0}^{t_1} dt_2\int_{t_0}^{t_2} dt_3\int_{t_0}^{t_3} dt_4 \\ \times\, e^{i[(\omega_x+\omega_{dc})t_1+(\omega_{bd}-\omega_x)t_2+(\omega_{ca}-\omega_y)t_3+(\omega_y+\omega_{ab})t_4-(\omega_f+\omega_{cd})(t-\tau))]}\end{aligned} \tag{B15}$$

The time integrals can be done by following the standard integral

$$\int_{-\infty}^{k} dt'\, e^{i\omega_{mn}t'} = \lim_{\Gamma_{mn}\to 0}\frac{ie^{i\omega_{mn}k}}{(\omega_{mn} - i\Gamma_{mn})} \tag{B16}$$

These integrals correspond to the Greens functions discussed in rule 2. Here Γ_{mn} is interpreted as the inverse lifetime of the transition $m \to n$. By taking $t_0 \to \infty$ and simplifying S^{el}_1, we get

$$\begin{aligned}S^{el}_1(\omega_f) = -2\Re \sum_{ss'gg'}\sum_{xy}\sum_{abcde} T^x_{s'}T^{x*}_s T^y_g T^{y*}_{g'}\frac{\rho_{aa}|V_{de}|^2}{\tilde{\omega}_{ab}\tilde{\omega}_{cb}\tilde{\omega}_{cd}\tilde{\omega}_{de}} \\ \times \frac{1}{i\Gamma}c^{\dagger}_{g,ab}c_{g',ca}c_{s,bd}c^{\dagger}_{s',dc}g(f_x\tilde{f}_y + f_y\tilde{f}_x + f_x\bar{f}_x + f_y\bar{f}_y)\end{aligned} \tag{B17}$$

where

$$\tilde{\omega}_{ab} = \frac{1}{(\omega_y + \omega_{ab} - i\Gamma_{ab})} \qquad \tilde{\omega}_{cb} = \frac{1}{(\omega_{cb} - i\Gamma_{cb})} \tag{B18}$$

$$\tilde{\omega}_{cd} = \frac{1}{(\omega_{cd} + \omega_x - i\Gamma_{cd})} \qquad \tilde{\omega}_{de} = \frac{1}{(\omega_{de} - \omega_f - i\Gamma_{de})} \tag{B19}$$

We now assume the lead states form a continuum and replace the summation over lead states by integrations over lead energies. This allows us to include the density of states (Ω_ν) corresponding to the leads. We further assume that the tunneling coefficients are independent of energy. So we get

$$\begin{aligned}S^{el}_1(\omega_f) = -2\Im \sum_{ss'gg'}\sum_{abcde}\sum_{\nu,\nu'\in l,r}\int d\omega_x\,\Omega_x(\omega_x)\int d\omega_y\,\Omega_x(\omega_y) \\ \times\, T^{\nu}_s T^{\nu*}_{s'}T^{\nu'}_g T^{\nu'*}_{g'}\frac{\rho_{aa}|V_{de}|^2 c^{\dagger}_{g,ab}c_{g',ca}c_{s,bd}c^{\dagger}_{s',dc}}{\Gamma\tilde{\omega}_{ab}\tilde{\omega}_{cb}\tilde{\omega}_{cd}\tilde{\omega}_{de}} \\ \times\, (f_x\tilde{f}_y + f_y\tilde{f}_x + f_x\bar{f}_x + f_y\bar{f}_y)\end{aligned} \tag{B20}$$

The evaluation of eq B20 is far from a triviality. However, one can analytically evaluate the signal at zero temperature where there exists only unidirectional flow and no thermal effects ($f_l = 1$ and $f_r = 0$). Thermal effects are known to play an important role in affecting electron transfer processes[42] which in turn may affect the optical properties. However, due to analytical restrictions to evaluate a thermally affected optical signal eq B20, we invoke the zero temperature limit. A particular advantage of the zero temperature limit is that it allows identification of the ground state ($\rho_{aa} = 1$ can be achieved.) We point out that eq B20 can be numerically evaluated using some mathematical form of the lead density of states to obtain a thermally affected electroluminescent signal. We are however interested in analytical evaluation and reduction of computational costs. So, in the zero temperature limit, we have

$$\begin{aligned}S^{el}_1(\omega_f) = -2\Im \sum_{ss'gg'}\sum_{\nu,\nu'\in l,r}\sum_{abcde} T^{\nu}_s T^{\nu'*}_{s'}T^{\nu}_g T^{\nu'*}_{g'} \\ \times \frac{\rho_{aa}|V_{de}|^2 c^{\dagger}_{g,ab}c_{g',ca}c_{s,bd}c^{\dagger}_{s',dc}}{\Gamma\tilde{\omega}_{de}\tilde{\omega}_{cb}} \\ \times \int d\omega_x \frac{\Omega_x}{\omega_{cd} - \omega_x - i\Gamma_{cd}}\int d\omega_y \frac{\Omega_y}{\omega_{ab} + \omega_y - i\Gamma_{ab}}\end{aligned} \tag{B21}$$

A realistic quantity is the derivative of the signal with respect to external bias. The bias eV in molecular junctions is analogous to an incoming excitation field in conventional spectroscopy. We use $\mu_l = \mu_0 + eV$ and $\mu_r = \mu_0$ and assume $\mu_0 = 0$. We differentiate the preceding signal with respect to external bias to get

$$\begin{aligned}\frac{d}{deV}S^{el}_1(\omega_f) = -2\Im \sum_{ss'gg'}\sum_{\nu,\nu'\in l,r}\sum_{abcde} T^{\nu}_s T^{\nu*}_{s'}T^{\nu'}_g T^{\nu'*}_{g'} \\ \times \frac{\rho_{aa}|V_{de}|^2 c^{\dagger}_{g,ab}c_{g',ca}c_{s,bd}c^{\dagger}_{s',dc}}{\tilde{\omega}_{de}\tilde{\omega}_{cb}} \\ \times \frac{\Omega_\nu(eV)}{\omega_{cd} + eV - i\Gamma_{cd}}\int_{-\infty}^{0} d\omega_x \frac{\Omega_{\nu'}(\omega_x)}{\omega_{ab} - \omega_x - i\Gamma_{ab}}\end{aligned} \tag{B22}$$

The differentiation with respect to bias gives the eV dependence in the first inward interaction (rule 4). Assuming a slowly varying density of states, we can make use of the integral

DOI: 10.1021/acs.jctc.5b00500
J. Chem. Theory Comput. 2015, 11, 4304−4315

$$\lim_{\Gamma\to 0}\int_0^\infty d\vartheta\ \frac{\Omega_i(\vartheta)}{(\chi+\vartheta-i\Gamma)}=\int_0^\infty d\vartheta\ \Omega_i(\vartheta)\ \delta(\chi+\vartheta)=\Omega_i(\chi) \tag{B23}$$

We get

$$\frac{d}{deV}S_1^{el}(\omega_f)=-2\Im\sum_{ss'gg'}\sum_{\nu,\nu'\in l,r}\sum_{abcde}T_s^{\nu}T_s^{\nu'*}T_g^{\nu}T_{g'}^{\nu'*}\times\frac{\rho_{aa}|V_{de}|^2c^{\dagger}_{g,ab}c_{g',ca}c_{s,bd}c^{\dagger}_{s',dc}}{\Gamma\tilde{\omega}_{de}\tilde{\omega}_{cb}}\frac{\Omega_\nu(eV)\,\Omega_{\nu'}(\omega_{ab})}{\omega_{cd}+eV-i\Gamma_{cd}} \tag{B24}$$

This integral gets rid of the first outward interaction as discussed in rule 3. We assume that the density of states is independent of energy (wide band approximation) and is equal in left and right leads. Now we get

$$\frac{d}{deV}S_1^{el}(\omega_f)=-2\Im\sum_{ss'gg'}\sum_{\nu,\nu'\in l,r}\sum_{abcde}\frac{T_{s'}^{\nu}T_s^{\nu'*}T_g^{\nu}T_{g'}^{\nu'*}}{\Gamma(\omega_{de}-\omega_f-i\Gamma_{de})}\times\frac{2\rho_{aa}\Omega^2|V_{de}|^2c^{\dagger}_{g,ab}c_{g',ca}c_{s,bd}c^{\dagger}_{s',dc}}{(\omega_{cb}-i\Gamma_{cb})(\omega_{cd}+eV-i\Gamma_{cd})} \tag{B25}$$

This expression is identical to eq 11 if one writes the frequency dependences in terms of the Greens function. Similar steps can be followed for all of the diagrams to evaluate the full signal. The same result for the signal is obtained by reading the ladder diagrams directly following the subsequently mentioned rules.

(1) Each interaction with an operator A contributes a matrix element of the type $\langle m|A_k|n\rangle = A_{k,mn}$. The many-body state m (n) corresponds to the state after (before) the interaction. On the ket (bra) side, these are written down from top to bottom (bottom to top). For example, in Figure 4, the interaction at time t_4 contributes as $\hat{c}^{\dagger}_{g,ab}$ while the one at t_3 contributes as $\hat{c}_{g',ca}$.

(2) Each time evolution from bottom to top in the ladder diagram is represented by a system Greens function which depends only on the energies of the states involved during that specific evolution and is defined as

$$\mathcal{G}(\omega_{mn})=\frac{i}{\omega_{mn}-i\Gamma_{mn}} \tag{B26}$$

Γ_{mn} is the inverse lifetime of the excitation $m\to n$, and $\omega_{mn}=\omega_m-\omega_n$ is the energy difference between the involved states.

(3) The evolution starting from the first outward interaction does not contribute to the signal.

(4) The Greens function corresponding to the first inward interaction has an additional energy dependence due to the applied bias, $\mathcal{G}(\omega_{mn}\pm eV)$. For the left (right) branch, the sign on eV is − (+).

(5) The Greens function in the final evolution gets an extra frequency dependence of the detected signal, $\mathcal{G}(\omega_{de}-\omega_f)$ such that $|d\rangle\to|e\rangle$ is the detected transition. Each lead interaction brings in a factor of molecule−lead coupling coefficient.

(6) The full signal is equal to twice the real part of the product of all of the preceding factors and square of the lead density of states.

In section III, we used these rules to write down the contribution from the ladder diagram shown in Figure 4i.

AUTHOR INFORMATION

Corresponding Authors

*(H.P.G.) E-mail: himangshu@ipc.iisc.ernet.in.

*(U.H.) E-mail: uharbola@ipc.iisc.ernet.in.

Funding

H.P.G. acknowledges the financial support from the University Grants Commission, New Delhi, India, under the Senior Research Fellowship scheme. S.M. gratefully acknowledges the support of the National Science Foundation (NSF) through Grant No. CHE-1361516 and from Chemical Sciences, Geosciences, and Biosciences Divison, Office of Basic Energy Sciences, Office of Science, (U.S.), Department of Energy (DOE). U.H. acknowledges support from the Indian Institute of Science, Bangalore, India.

Notes

The authors declare no competing financial interest.

ACKNOWLEDGMENTS

H.P.G. thanks Dr. Bijay K. Agarwalla for helpful discussions.

REFERENCES

(1) Breuer, H. P.; Petruccione, F. *The theory of open quantum systems*, 1st ed.; Oxford University Press: Oxford, U.K., 2002; pp 109−171.

(2) Weiss, U. *Quantum dissipative systems*, Vol. 13, 3rd ed.; World Scientific: Singapore, 2008; pp 5−56.

(3) Sun, L.; Diaz-Fernandez, Y. A.; Gschneidtner, T. A.; Westerlund, F.; Lara-Avila, S.; Moth-Poulsen, K. Single-molecule electronics: from chemical design to functional devices. *Chem. Soc. Rev.* **2014**, *43*, 7378−7411.

(4) Stipe, B. C.; Rezaei, M. A.; Ho, W. Single-molecule vibrational spectroscopy and microscopy. *Science* **1998**, *280*, 1732−1735.

(5) Nazin, G. V.; Qiu, X. H.; Ho, W. Visualization and spectroscopy of a metal-molecule-metal bridge. *Science* **2003**, *302*, 77−81.

(6) Shamai, T.; Selzer, Y. Spectroscopy of molecular junctions. *Chem. Soc. Rev.* **2011**, *40*, 2293−2305.

(7) Tao, N. J. Electron transport in molecular junctions. *Nat. Nanotechnol.* **2006**, *1*, 173−181.

(8) Tian, J.-H.; Liu, B.; Xiulan; Yang, Z.-L.; Ren, B.; Wu, S.-T.; Nongjian; Tian, Z.-Q. Study of Molecular Junctions with a Combined Surface-Enhanced Raman and Mechanically Controllable Break Junction Method. *J. Am. Chem. Soc.* **2006**, *128*, 14748−14749.

(9) Abramavicius, D.; Palmieri, B.; Voronine, D. V.; Sanda, F.; Mukamel, S. Coherent multidimensional optical spectroscopy of excitons in molecular aggregates; quasiparticle versus supermolecule perspectives. *Chem. Rev.* **2009**, *109*, 2350−2408.

(10) Biggs, J. D.; Zhang, Y.; Healion, D.; Mukamel, S. Watching energy transfer in metalloporphyrin heterodimers using stimulated X-ray Raman spectroscopy. *Proc. Natl. Acad. Sci. U. S. A.* **2013**, *110*, 15597−15601.

(11) Sonntag, M. D.; Klingsporn, J. M.; Zrimsek, A. B.; Sharma, B.; Ruvuna, L. K.; Van Duyne, R. P. Nano plasmonics for nanoscale spectroscopy. *Chem. Soc. Rev.* **2014**, *43*, 1230−1247.

(12) Sukharev, M.; Seideman, T.; Gordon, R. J.; Salomon, A.; Prior, Y. Ultrafast Energy Transfer Between Molecular Assemblies and Surface Plasmons in the Strong Coupling Regime. *ACS Nano* **2014**, *8*, 807−817.

(13) Parker, S. M.; Smeu, M.; Franco, I.; Ratner, M. A.; Seideman, T. Molecular junctions: can pulling influence optical controllability? *Nano Lett.* **2014**, *14*, 4587−4591.

(14) Zhitenev, N. B.; Meng, H.; Bao, Z. Conductance of small molecular junctions. *Phys. Rev. Lett.* **2002**, *88*, 226801.

(15) Chung, H. S.; Gopich, I. V. Fast single-molecule FRET spectroscopy: theory and experiment. *Phys. Chem. Chem. Phys.* **2014**, *16*, 18644−18657.

(16) Barkai, E.; Jung, Y.; Silbey, R. Theory of single-molecule spectroscopy: beyond the ensemble average. *Annu. Rev. Phys. Chem.* **2004**, *55*, 457−507.

(17) Mukamel, S. *Principles of Nonlinear Optical Spectroscopy*, 1st ed.; Oxford University Press: New York, 1999; pp 265.

DOI: 10.1021/acs.jctc.5b00500
J. Chem. Theory Comput. 2015, 11, 4304−4315

(18) Mukamel, S.; Tanimura, Y.; Hamm, P. Coherent multidimensional optical spectroscopy. *Acc. Chem. Res.* **2009**, *42*, 1207−1209.
(19) Marx, C. A.; Harbola, U.; Mukamel, S. Nonlinear optical spectroscopy of single, few, and many molecules: Nonequilibrium Green's function QED approach. *Phys. Rev. A: At., Mol., Opt. Phys.* **2008**, *77*, 022110.
(20) Rahav, S.; Mukamel, S. Multidimensional optical spectroscopy of a single molecule in a current-carrying state. *J. Chem. Phys.* **2010**, *133*, 244106.
(21) Harbola, U.; Agarwalla, B. K.; Mukamel, S. Frequency-domain stimulated and spontaneous light emission signals at molecular junctions. *J. Chem. Phys.* **2014**, *141*, 074107.
(22) Galperin, M.; Ratner, M. A.; Nitzan, A. Raman scattering from nonequilibrium molecular conduction junctions. *Nano Lett.* **2009**, *9*, 758−762.
(23) Galperin, M.; Nitzan, A. Current-induced light emission and light-induced current in molecular-tunneling junctions. *Phys. Rev. Lett.* **2005**, *95*, 206802.
(24) Harbola, U.; Maddox, J. B.; Mukamel, S. Many-body theory of current-induced fluorescence in molecular junctions. *Phys. Rev. B: Condens. Matter Mater. Phys.* **2006**, *73*, 075211.
(25) Galperin, M.; Ratner, M. A.; Nitzan, A. Inelastic electron tunneling spectroscopy in molecular junctions: Peaks and dips. *J. Chem. Phys.* **2004**, *121*, 11965−11979.
(26) Schubert, E. F. *Light emitting diodes*, 2nd ed.; Cambridge University Press: Cambridge, U.K., 2006; pp 1−56.
(27) Burroughes, J. H.; Bradley, D. D. C.; Brown, A. R.; Marks, R. N.; Mackay, K.; Friend, R. H.; Burns, P. L.; Holmes, A. B. Light-emitting diodes based on conjugated polymers. *Nature* **1990**, *347*, 539−541.
(28) Caruge, J. M.; Halpert, J. E.; Wood, V.; Bulovic, V.; Bawendi, M. G. Colloidal quantum-dot light-emitting diodes with metal-oxide charge transport layers. *Nat. Photonics* **2008**, *2*, 247−250.
(29) Marquardt, C. W.; Grunder, S.; Błaszczyk, A.; Dehm, S.; Hennrich, F.; Lohneysen, H. V.; Mayor, M.; Krupke, R. Electroluminescence from a single nanotube-molecule-nanotube junction. *Nat. Nanotechnol.* **2010**, *5*, 863−867.
(30) Yang, H.; Mayne, A. J.; Comtet, G.; Dujardin, G.; Kuk, Y.; Nagarajan, S.; Gourdon, A. Single-molecule light emission at room temperature on a wide-band-gap semiconductor. *Phys. Rev. B: Condens. Matter Mater. Phys.* **2014**, *90*, 125427.
(31) Beams, R.; Bharadwaj, P.; Novotny, L. Electroluminescence from graphene excited by electron tunneling. *Nanotechnology* **2014**, *25*, 055206.
(32) Uemura, T.; Yamaguchi, S.; Akai-Kasaya, M.; Saito, A.; Aono, M.; Kuwahara, Y. Tunneling-current-induced light emission from individual carbon nanotubes. *Surf. Sci.* **2006**, *600*, L15−9.
(33) Misewich, J. A.; Martel, R.; Avouris, Ph.; Tsang, J. C.; Heinze, S.; Tersoff, J. Electrically induced optical emission from a carbon nanotube FET. *Science* **2003**, *300*, 783−786.
(34) Reecht, G.; Scheurer, F.; Speisser, V.; Dappe, Y. J.; Mathevet, F.; Schull, G. Electroluminescence of a polythiophene molecular wire suspended between a metallic surface and the tip of a scanning tunneling microscope. *Phys. Rev. Lett.* **2014**, *112*, 047403.
(35) Harbola, U.; Mukamel, S. Superoperator nonequilibrium Greens function theory of many-body systems; applications to charge transfer and transport in open junctions. *Phys. Rep.* **2008**, *465*, 191.
(36) Reed, M. A.; Zhou, C.; Muller, C. J.; Burgin, T. P.; Tour, J. M. Conductance of a Molecular Junction. *Science* **1997**, *278*, 252−254.
(37) Agarwalla, B. K.; Harbola, U.; Hua, W.; Zhang, Y.; Mukamel, S. Coherent (photon) vs incoherent (current) detection of multidimensional optical signals from single molecules in open junctions. *J. Chem. Phys.* **2015**, *142*, 212445.
(38) Yaliraki, S. N.; Roitberg, A. E.; Gonzalez, C.; Mujica, V.; Ratner, M. A. he injecting energy at molecule/metal interfaces: Implications for conductance of molecular junctions from an ab initio molecular description. *J. Chem. Phys.* **1999**, *111*, 6997.
(39) Hirata, S.; Head-Gordon, M. Time-dependent density functional theory within the Tamm-Dancoff approximation. *Chem. Phys. Lett.* **1999**, *314*, 291−299.
(40) Valiev, M.; Bylaska, E.; Govind, N.; Kowalski, K.; Straatsma, T.; Van Dam, H.; Wang, D.; Nieplocha, J.; Apra, E.; Windus, T.; de Jong, W. NWChem: A comprehensive and scalable open-source solution for large scale molecular simulations. *Comput. Phys. Commun.* **2010**, *181*, 1477−1489.
(41) Zhang, Y.; Biggs, J. D.; Healion, D.; Govind, N.; Mukamel, S. Core and Valence Excitations in Resonant X-ray Spectroscopy Using Restricted Excitation Window Time-Dependent Density Functional Theory (REW-TDDFT). *J. Chem. Phys.* **2012**, *137*, 194306.
(42) Goswami, H. P.; Harbola, U. Electron transfer statistics and thermal fluctuations in molecular junctions. *J. Chem. Phys.* **2015**, *142*, 084106.

DOI: 10.1021/acs.jctc.5b00500
J. Chem. Theory Comput. 2015, 11, 4304−4315